ARCHIVES OF CIVIL AND MECHANICAL ENGINEERING 16 (2016) 734–742

Available online at www.sciencedirect.com

ScienceDirect

journal homepage: http://www.elsevier.com/locate/acme

Original Research Article

Chloride-induced corrosion modelling of cracked reinforced SHCC

Suvash C. Paul [a,b,*], Gideon P.A.G. van Zijl [b,1]

[a] Singapore Centre for 3D Printing, School of Mechanical and Aerospace Engineering, Nanyang Technological University, Singapore

[b] Department of Civil Engineering, Stellenbosch University, South Africa

ARTICLE INFO

Article history:
Received 4 January 2016
Accepted 29 April 2016
Available online 1 June 2016

Keywords:
Chloride
Cracks
Corrosion modelling
Pitting depth
Strain hardening cement-based composite (SHCC)

ABSTRACT

Corrosion of steel bars in concrete is usually a slow electrochemical process which may need a long time before damage becomes visible in the reinforced concrete (RC). However, cracks provide quick access to chloride, oxygen and water into concrete and accelerate the corrosion process. Corrosion modelling is essential for structural design for a particular life span, or to inform decisions on repair of RC structures to reach or extend their service life. This paper reports experimental research results of accelerated chloride exposure of cracked reinforced strain hardening cement-based composite (R/SHCC) specimens for a period of one year. Based on these novel results, a corrosion model is proposed which incorporates crack width, crack spacing, free chloride content and cover depth. The model is shown to capture the corrosion results of cracked R/SHCC reported in this paper.

1. Introduction

At present there is no corrosion model for strain hardening cement-based composite (SHCC), a relatively new construction material. Existing corrosion models for reinforced concrete (RC) are open to criticism due to the fact that they in some cases over-estimate, and in other cases under-estimate actual corrosion [1]. Corrosion is a complex deterioration mechanism and there is no direct way to determine the actual corrosion rate. Also, most prediction models for chloride-induced corrosion in RC generally assume uncracked concrete, while design standards generally allow cracks, but limit crack widths in service conditions. These models typically enable estimation of (i) the time for sufficient concentration levels of chloride to reach reinforcing steel in RC to cause corrosion initiation [2] and (ii) the time for corrosion-induced cracks to appear on concrete surface [3]. The time to corrosion cracking is determined by considering the time dependent pressure build-up caused by corrosion products in the surrounding concrete, including refined consideration for impregnation of the porous interfacial zone surrounding the steel.

A third category of corrosion models could be considered for the corrosion rate in cracked RC. This is the most complicated category, which is probably the reason why

* *Corresponding author*. Tel.: +65 6790 4000.
E-mail addresses: suvashpl@ntu.edu.sg (S.C. Paul), gvanzijl@sun.ac.za (G.P.A.G. van Zijl).
[1] Tel.: +27 21 808 4369; fax: +27 21 808 4440.

http://dx.doi.org/10.1016/j.acme.2016.04.016
1644-9665/

limited modelling attempts have been reported [4,5]. Typically, cracks act as pathways for ingress of chlorides, which de-passivates the steel in concrete, causing dissolution of iron into the pore water. Ingress of water and oxygen, either via the crack or through the cover concrete, forms the cathode of the electrochemical corrosion cell by formation of hydroxyls in close vicinity of the anode in the crack zone or at passive steel further away in uncracked regions. It is generally believed that the probability of corrosion is increased with increased crack width [6], which is the background of crack width limitation by design standards for durability of RC. However, light was shed on the importance of crack spacing by Arya and Ofori-Darko [7] for corrosion rate in RC.

In the type 1 models as categorised above, corrosion initiation is considered to occur once a threshold level of free chloride is present at the steel surface in RC [3,8]. However, a range of threshold limit values have been reported by various authors, e.g. Mohammed et al. [4], Huang [9] and Alonso et al. [10]. The chloride threshold appears to depend on several factors including the exposure conditions [11], the concrete mix design [12] and the binder composition [13]. Since the matrix properties of SHCC are different from that of traditional concrete types, the chloride threshold level in SHCC may differ. The published data on chloride content and profiles in SHCC is limited [14].

There is no existing evidence that the corrosion rate is dependent on chloride content. This motivates the investigation of chloride content, as well as crack width and spacing in this paper, towards deriving a type 3 model for corrosion rate in cracked R/SHCC. A coulostatic method is used to measure the corrosion rate in the steel bar [15–17]. Accelerated chloride-induced corrosion testing was performed by exposure to a 3.5% NaCl aqueous solution for 3 days, followed by 4 days of drying, in regular weekly cycles for total durations of 28–57 weeks.

2. Research significance

The corrosion rate in SHCC class materials has been studied by the several researchers [17–20]. None of these researchers attempted to correlate the crack patterns or chloride content and corrosion rate or damage. In chloride-induce corrosion, the corrosion current is influenced by the position and relative size of the anodic and cathodic areas [21]. Therefore, the crack spacing may be important in separation of anodic and cathodic areas. It is postulated that, in a specimen containing a single crack, a large cathodic area allows a large amount of ions to move from the cathode to the anode. Due to the resulting high corrosion current in this macro-cell corrosion, deeper pitting corrosion depths may be expected in the steel bar in the vicinity of the anode. Multiple cracks distribute the anodic and cathodic areas over the steel bar, whereby the cathode to anode area ration significantly reduces. In this micro-cell corrosion the corrosion current is reduced and a low corrosion rate is expected [21,22]. This study is novel in presenting free and total chloride content in cracked R/SHCC, coulostatic measurement of corrosion rates and actual corrosion damage quantification, as well as correlating the measured and actual corrosion damage with chloride content, crack width and crack spacing. The corrosion rate may be influenced by several other factors, including the concrete temperature, pH, resistivity and availability of oxygen [23]. However, in the novel chloride-induced corrosion model for R/SHCC proposed by this paper, the focus is on chloride content and the crack pattern, while other factors considered to be less dominant are kept in mind in interpretation of corrosion current results.

3. Experimental program

The mix proportions of the SHCC used here are summarised in Table 1. It contained finely grained sand with maximum particle size of 0.30 mm and fineness modulus (FM) 1.9, and two volume percent of Polyvinyl alcohol (PVA) fibres with length 12 mm and diameter 0.04 mm. Characterisation of the SHCC was done by testing 100 mm cubes for compressive strength and small dumbbell shaped specimens with gauge region of 16 mm × 30 mm cross-section and 80 mm long for uniaxial tensile behaviour. The cubes were tested at the age of 28 days while reinforced beams and unreinforced dumbbell specimens were tested at 14 days. Two days after casting, all specimens were removed from their moulds and cured in water at 21 ± 2 °C for 7 days, and subsequently in a laboratory environment of 21 ± 2 °C and relative humidity (RH) 55 ± 5% until the testing date.

3.1. *Specimen preparation for corrosion testing of R/SHCC*

For R/SHCC corrosion testing of two series of SHCC specimens denoted by FS31 and FS32, 80 mm × 100 mm × 490 mm beams were used. A 10 mm diameter steel bar (denoted Y10) and 500 mm length was placed inside the beams at three different cover depths. In total 18 FS31 specimens were prepared, with as parameters the cover depth (15, 25 and 35 mm) and pre-cracking (in a three-point bending) deflection (5 and 7 mm), with three specimens of each type. Note that these deflection levels also represent the ultimate load capacity of these R/SHCC specimens, chosen to produce significant crack widths. After unloading, each FS31 specimen was placed in a specially prepared steel frame shown in Fig. 1a, in which the 5 and 7 mm central deflections respectively were re-applied by tightening the nuts onto the bolts at both ends of the specimens. These levels of deformation were maintained in the frames. Several

Table 1 – Mix proportions of different SHCC.

Type	Id	Cement	Water	Fly-ash	Sand	Fibre (%)
SHCC	FS31/FS32	1 (CEM I 52.5)	1.0	1.72	1.41	2.0

Note that superplasticizer and viscosity modifying agents were added to achieve the correct fresh properties of the SHCC.

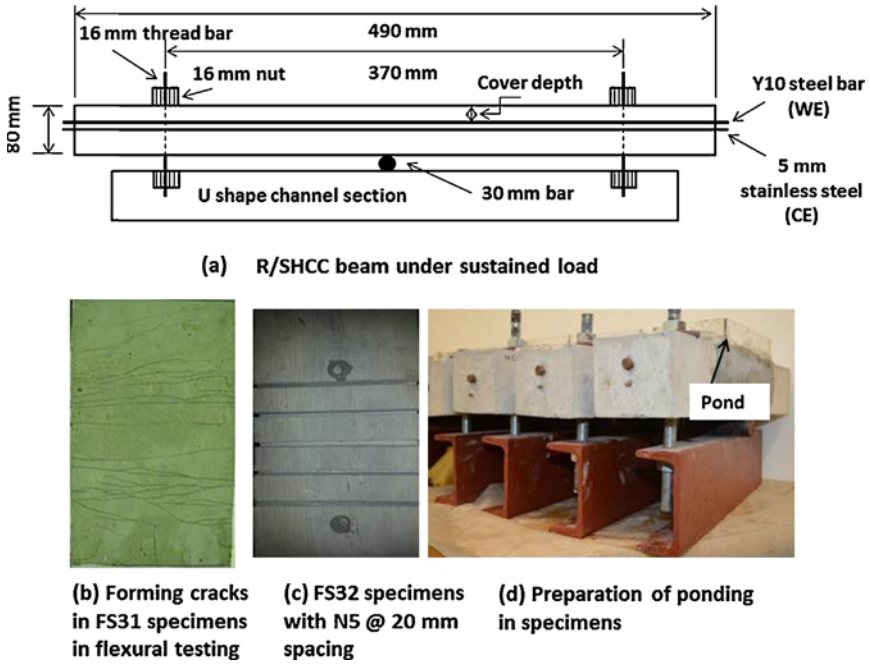

Fig. 1 – R/SHCC specimen preparation for corrosion testing.

cracks were found on the tensile face of each specimen (see Fig. 1b).

In total 18 FS32 specimens were prepared, also with a single Y10 steel bar at 2 cover depths (15 and 25 mm) and 3 crack spacings (a single central crack (N1), 3 cracks space 40 mm apart (N3), 5 cracks spaced 20 mm apart (N5)), with 3 specimens of each type. The crack spacing was enforced by cutting notches 10 mm deep and 3 mm wide in the tensile face in the central part of the specimens as shown in Fig. 1c. The specimens were placed in similar steel frames as the FS31 specimens and cracks were formed by tightening the nuts on the bolts at the frame ends. In this case the specimens were loaded up to a certain tensile surface deformation level measured over a gauge length of 100 mm over the notched region. For 1, 3 and 5 notches the surface elongation was 0.30 mm, 0.90 mm and 1.5 mm respectively in order to create cracks in the notches of roughly equal widths.

In each FS31 and FS32 specimen a 6 mm stainless steel bar of the same length as the Y10 reinforcing bar was also placed (see Fig. 1a) as counter electrode for coulostatic measurements. A pond of nominal size 200 mm × 100 mm was built on each specimen's cracked surface (Fig. 1d) from non-absorbent plastic, sealed with silicon. 3.5% (by weight) NaCl aqueous solution was poured into this pond for the 3 day wetting part of the cyclic exposure, after which the solution was removed for 4 days of drying. FS31 were exposed to 57 weeks of these cycles, and FS32 specimens to 28 weeks FS32. The sides of the FS31 and FS32 specimens were sealed to prevent moisture loss through these faces.

3.2. *Method of corrosion measurement of R/SHCC*

A coulostatic method [15,16] was used to measure the steel corrosion rate. In this method, the polarisation resistance (R_p) of the concrete was calculated from the $\Delta I/\Delta E$ ratio, where ΔI is a small, known current applied to the specimen and ΔE is the potential decay in the specimen. The steel reinforcing bar acted as the working electrode (WE) and the smooth 6 mm diameter stainless steel bar acted as the counter electrode (CE). A Ag/AgCl half-cell was used as the reference electrode. For the corrosion rate measurement, a Spider8 data logger was used while a current of 4 mA was applied to each of the specimens for a period of 5 ms by a laboratory built current pulse generator. However, for six FS31 specimens with a cover depth of 15 mm a different current of 10 mA for a period of 6 ms was used. The reason was the low perturbation with the usual current spike (4 mA for 5 ms) in these specimens. A suitable perturbation and decay vs time curve could not be obtained with the lower current in these specimens. It may be because of the larger total crack widths in these specimens resulting in more easy access of water and oxygen to the steel influencing the concrete resistivity, since this plays a significant role when the current is applied to the steel bar [21,23]. As a result a higher value of current was applied for a slightly longer time period to these six specimens. From the corrosion rate (V_{corr}) results, Eq. (1) was used to estimate uniformly corroded depth (d_c) in the steel bars as follows:

$$d_c(t) = d_{c0} + \int_0^t V_{corr}\,dt = d_{c0} + \sum_{i=1}^{N_t} \frac{1}{2}(V_{corr} + V_{corr,i-1})(t_i - t_{i-1}) \quad (1)$$

After the accelerated corrosion testing, some of the specimens were broken to observe actual corrosion in the steel bars.

3.3. *Method of determining chloride content in R/SHCC*

In order to study the chloride penetration into the cracked specimens after the cyclic exposure, a total of 20 R/SHCC

specimens were chosen from both types (FS31, FS31). For this purpose, drilling was performed to collect powder samples from the drilling residue. A 16 mm diameter drill was used. Layers depths of 3 mm each were drilled at four to six crack positions to ensure sufficient powder per layer. So, the chloride content obtained here is one dimensional (depth) and the average value of different positions at that layer depth. All the drilling positions were into cracks. X-ray fluorescence (XRF) testing was performed to determine the total chloride content. Chemical analysis was also performed, both for total and free chloride content in each layer. In the case of chemical analysis, the RILEM TC 178-TMC [24,25] recommendations were followed.

3.4. *Method of determining pitting depths of corroded steel bars of R/SHCC*

After corrosion testing up to specified periods, all the specimens were broken and the steel bars were collected and cleaned with hydrochloric acid (HCl) and a wire brush. Subsequently, the pitting depths were measured using a dial gauge with a 10 μm resolution. Although many shallower pitting depths could be seen in most steel bars, three to six representing pitting regions were selected, from which the average and maximum pitting depths were determined in each steel bar.

4. Experimental outcomes

The SHCC, the slump flow and air content were also measured. The range of slump flow was in the range 170–210 mm and air content 3–4.8%. The SHCC mechanical properties of compressive strength (f_{cu}), flexural strength ($f_{u,ft}$) and uniaxial tensile strength ($f_{u,st}$) determined from smaller specimens are summarised in Table 2.

4.1. *Flexural cracking behaviour of R/SHCC*

The average number of flexural cracks, surface crack widths and their spacing in R/FS31 specimens are shown in Fig. 2a–d. Note that this figure is only for 5 mm level of deformation of specimens. In all specimens, most crack widths were in the range of 50–100 μm, but a few crack widths were also found to

Table 2 – Mechanical properties of different SHCCs.

Id	Strength (MPa)			E-Modulus (GPa)	Ultimate flexural deformation (mm)	Ultimate tensile strain (%)
	f_{cu}	$f_{u,ft}$	$f_{u,st}$			
FS31 and FS32	23–24	7–9	2.2–2.8	13–14	3–4	2–2.2

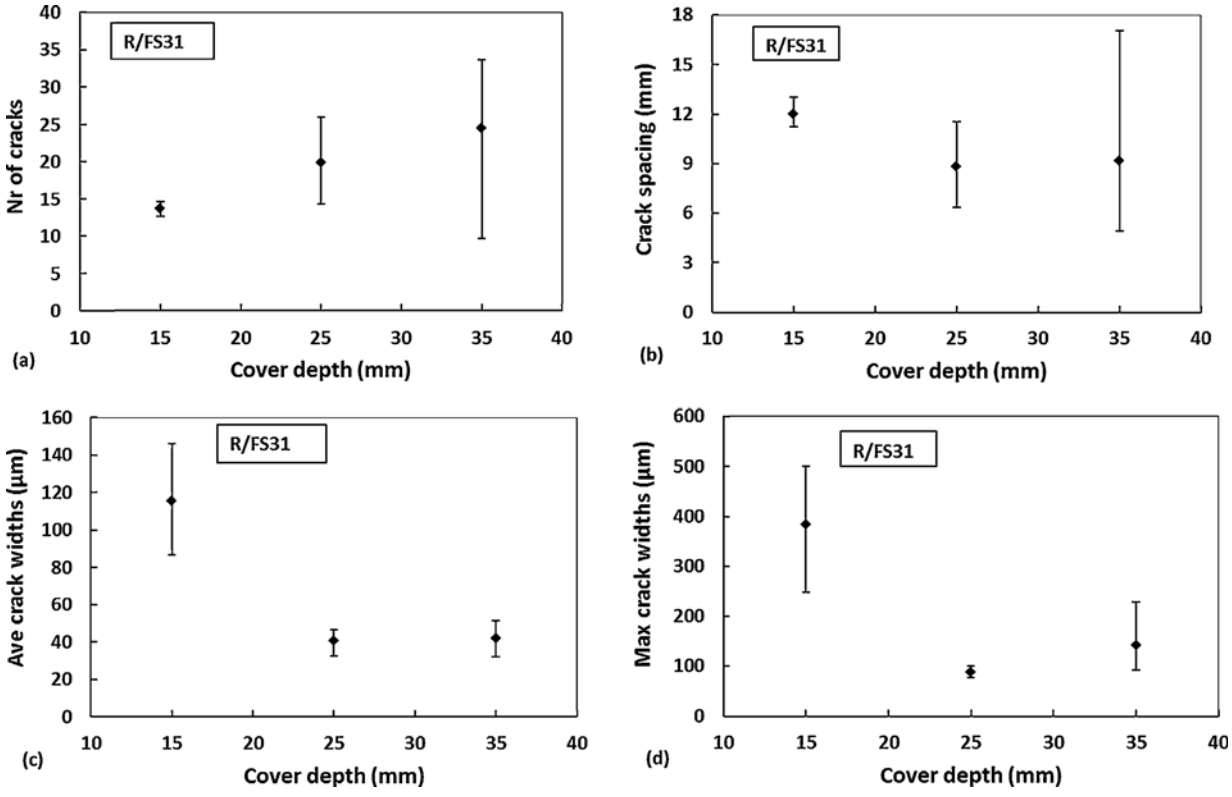

Fig. 2 – Flexural cracking behaviour at different cover depths of R/FS31 specimens at 5 mm deformation level.

Table 3 – Empirical formula obtained from R/SHCC in flexural testing.

Parameters	Obtained relationship	Regression factor (R^2)
Nr of crack (N_{cr}) vs cover depth (C) (mm)	$N_{cr} = 4.94C^{0.423}$	0.98
Ave crack widths ($W_{cr,ave}$) (μm) vs cover depth (C) (mm)	$W_{cr,ave} = 733.5C^{-0.845}$	0.85
Crack spacing (S_{cr}) (mm) vs cover depth (C) (mm)	$S_{cr} = 20.18C^{-0.24}$	0.74

be in the range of 100–200 μm especially in specimens with 15 mm cover. An insignificant difference in the number of cracks was found in R/FS31 due to the increased deflection from 5 mm to 7 mm. It may be due to the fact that all the specimens had reached their ultimate level of resistance after about 3 mm, at which point crack saturation was most likely reached. Deflection beyond this point typically leads to increased crack widths, instead of the formation of more cracks.

Average crack spacing in Fig. 2b was calculated by dividing the total number of cracks limited to the central 180 mm of each specimen into this length. The crack spacing was generally larger in the specimens with 15 mm cover depth (C15). For the particular SHCC specimens used here, it was found that there was no major difference in the number of cracks, and the crack spacing between the C25 and C35 specimens. The higher number of cracks for larger cover depth in SHCC specimens may be explained by the role of the steel bar ribbed deformations in determining the crack spacing, as can be observed in the results of Fischer and Li [26]. At higher cover, the influence of the steel bar ribs is reduced, and the intrinsic crack spacing of the particular SHCC reappears.

Table 3 shows the empirical relationships obtained from the results in Fig. 2a–d. Note that in the R/FS32 specimens the surface crack widths could not be measured, but taken from the surface elongation during the pre-cracking of each specimen. The number of cracks and crack spacing in R/FS32 specimens are those of the respective number and spacing of the notches described in Section 3.1.

4.2. *Corrosion behaviour of R/SHCC*

The chloride-induced corrosion damage in the steel bars in the R/FS31 specimens are reported as the corroded depths calculated with Eq. (1), pitting depths, as well as total and free chloride contents at the steel bar surface in this section.

4.2.1. *Cracks and corroded depth in R/SHCC*

The corroded depths of R/FS31 specimens after 57 weeks of accelerated testing are shown in Fig. 3a and b in terms of

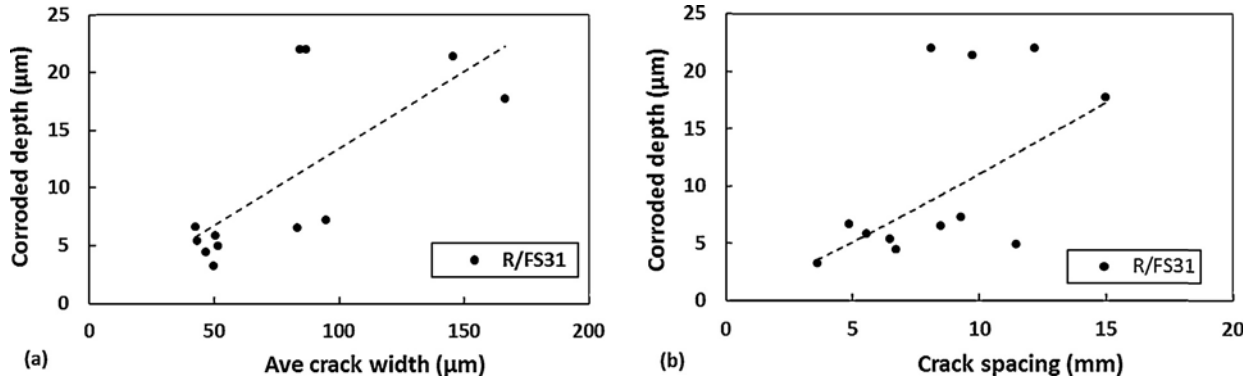

Fig. 3 – Influence of crack widths and spacing on corroded depths in R/FS31 specimens after 57 weeks of cyclic chloride exposure.

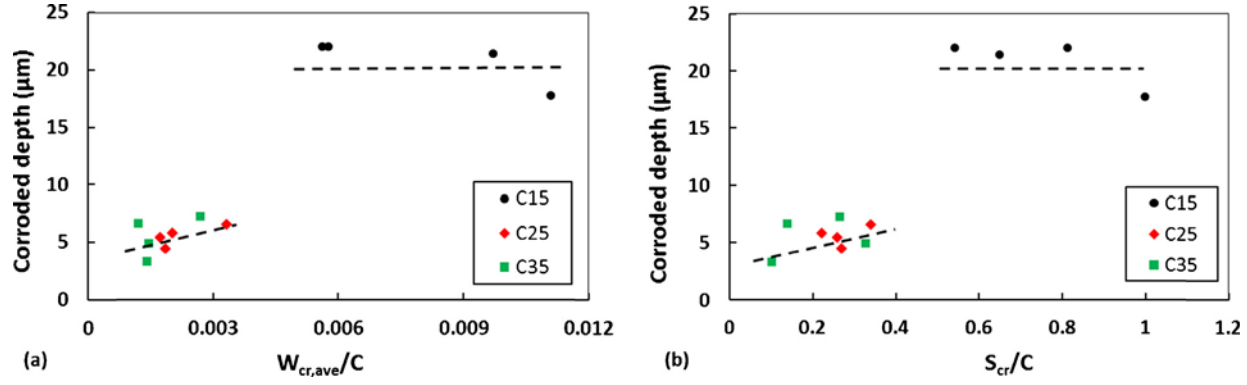

Fig. 4 – Relationship between the corroded depths calculated from corrosion rate readings with Eq. (1) and (a) average crack widths/cover depth ($W_{cr,ave}/C$) and (b) crack spacing/cover depth (S_{cr}/C) in R/FS31 specimens after 57 weeks of cyclic chloride exposure.

average crack widths and spacing. It appears that larger corroded depths occur in specimens with larger average crack widths, and also for larger crack spacing in these specimens. It must be kept in mind that these results are for the different cover depths in the R/FS31 specimens. In Fig. 4a and b distinction is made between the cover widths, showing significantly higher corroded depths for the C15 specimens. It appears that a threshold cover depth of roughly 25 mm exists for these specimens, beyond which insignificant difference in corroded depth is found. The reason could be the (i) different currents in the coulostatic measurement of the corrosion rate in the C15 specimens as mentioned in Section 3.2, and (ii) the wider cracks spaced further apart (Fig. 2b–d).

4.2.2. *Cracks and pitting in R/SHCC*

The average pitting corrosion depths in the individual steel bars were found to be higher for larger crack spacing in the R/FS31 specimens as shown in Fig. 5. It may be explained by the larger number of cracks and thus closer average crack spacing, which led to dominantly micro-cell corrosion. Macro-cell corrosion causes more severe pitting depths than micro-cell corrosion [21]. Here, more distributed corrosion was found in the steel bars. A larger number of cracks spaced closer together led to lower pitting corrosion depths, as shown in the near linear trend in Fig. 5. This is considered to be in agreement with the report by Schiessl and Raupach [27] that an increase in crack spacing in RC from 10 to 20 cm causes the corrosion rate to double. It is acknowledged that total mass loss would be a more direct measure of steel bar corrosion damage, and will be measured carefully in future work.

4.3. *Chloride profile in R/SHCC*

In order to study the dependence of the level of corrosion damage on chloride content, chloride profiling was done for all specimens. Chloride content was determined by both XRF and chemical testing, and is reported as the percentage of binder (cement and fly-ash) weight in this section. The relationship between the total chloride determined by XRF and chemical testing is shown in Fig. 6. A strongly correlated linear relationship is found between the XRF and chemical test results, which confirms that XRF, a much simpler and quicker process, is an alternative method for determining total chloride content in cement-based composites.

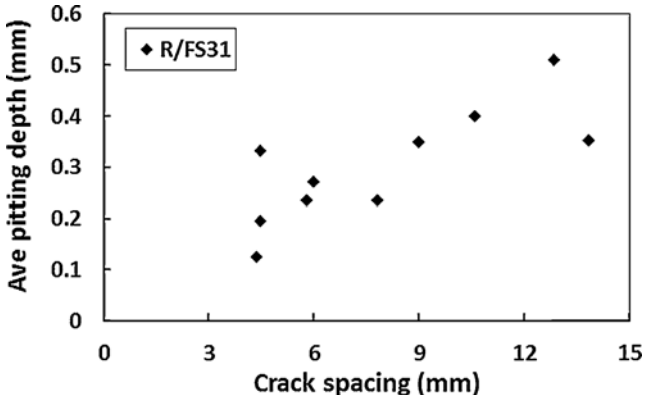

Fig. 5 – Average pitting depths vs crack spacing in R/FS31 specimens at the end of their exposure periods.

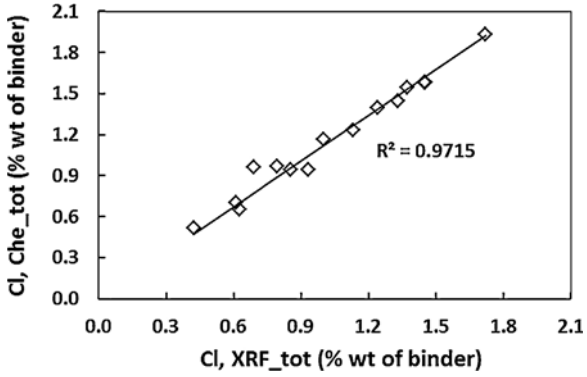

Fig. 6 – Relationship between total chloride (Cl) content obtained by XRF and chemical testing.

4.3.1. *Total and free chloride in R/SHCC*

Fig. 7a and b shows typical total and free chloride profiles in cracked R/FS31 and R/FS32 specimens, determined by chemical titration. Note that because of time constraints, these chloride profiles were not determined in all the specimens. However, total chloride profiles were determined by XRF in 15 specimens from both SHCC types, since the XRF testing method is significantly quicker [28]. The typical trend of high chloride content close to the exposed surface and gradual reduction with depth is seen in the figures. From the results

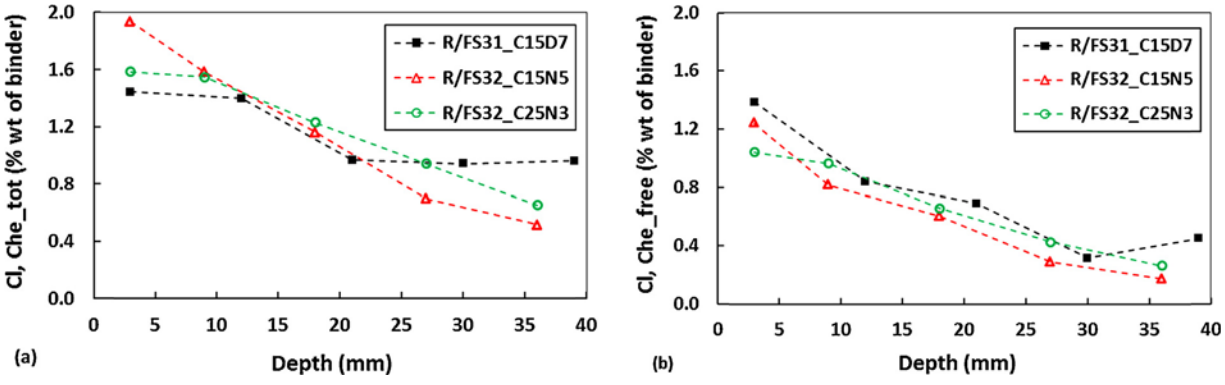

Fig. 7 – (a) Total and (b) free chloride profiles in different R/SHCC specimens.

found in this research the maximum total and free chloride content for was about 2% and 1.4% of the binder weight respectively.

Fig. 8 shows relationships between the corroded depths determined by the coulostatic method (Eq. (1)) and total and free chloride contents at the surface of steel bars in the different R/SHCC specimens. A better correlation is seen between corroded depth and free chloride content, suggesting that free chloride content might be more relevant for the corrosion activity.

4.3.2. *Relationship between cracks, corrosion and chloride in R/SHCC*

In Fig. 9 total chloride content at the steel bar surface is plotted against average crack width per specimen. A dashed line is fitted, indicating a trend of higher chloride content for higher average crack widths. It must be kept in mind that these chloride contents were found after 57 weeks of cyclic chloride exposure. This would allow time for chloride to migrate deep into cracks and subsequently into the surrounding matrix [28] also included in the drilled samples for chloride profiling. Djerbi et al. [29] and Boshoff et al. [30] reported threshold crack widths of 30 μm below which no chloride diffusion was found, and 100 μm beyond which crack width constant chloride diffusion was observed in water-filled, parallel-faced cracks in both ordinary concrete and fibre reinforced concrete. They reported a linear relation between these two threshold crack widths. It is clear that the steady-state chloride diffusion [29] is different from the conditions here, where chloride accumulated in flexural cracks during 57 weeks of cyclic exposure. It is nevertheless postulated that an initially linear relation between chloride content and crack width may be expected, with an eventual flattening trend of the total accumulated chloride content with crack width as indicated by the trendline in Fig. 9.

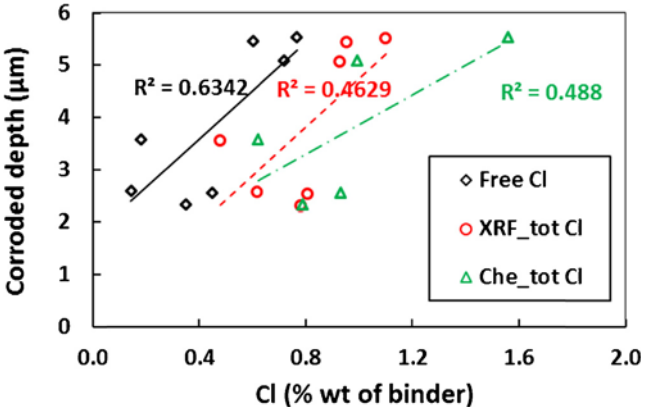

Fig. 8 – Relationship between total and free chloride contents at the steel bar surface with corroded depths.

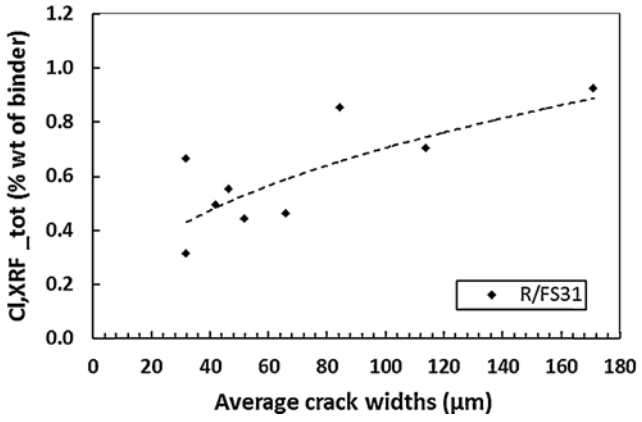

Fig. 9 – XRF total chloride (Cl) and average crack widths relationship in R/SHCC specimens after 57 weeks of chloride exposure.

5. Corrosion modelling of R/SHCC

To date, no corrosion model for cracked R/SHCC exposed to chloride has been proposed in the literature. In the existing corrosion models for RC, different parameters were considered by the different researchers. As a result, the results obtained from these corrosion models vary significantly. Due to limited corrosion data on SHCC, validation of these models, or one proposed here for R/SHCC is not possible, and more, long term research and monitoring of actual structures are required in this regard. In this section, the data sets generated in the research reported here are used to propose a model.

5.1. *Proposed corrosion modelling of R/SHCC*

From the relationships shown in Section 4 between corrosion and crack width, crack spacing, cover depth and chloride content, the following two relations have been derived:

$$d_c = \frac{\delta_T \delta_{RH} W_{cr,ave} t^{\alpha_t} Cl_{free}^{\alpha_{cl}}}{C^{\alpha_C}} \quad \text{for R/SHCC containing a single crack} \tag{2}$$

$$d_c = \frac{0.35 \delta_T \delta_{RH} W_{cr,ave} t^{\alpha_t} Cl_{free}^{\alpha_{cl}} S_{cr}^{\alpha_S}}{C^{\alpha_C}} \quad \text{for R/SHCC containing multiple cracked} \tag{3}$$

where d_c is the corroded depth (μm), t is the corrosion time (year), $W_{cr,ave}$ is the average crack width in the specimen (μm),

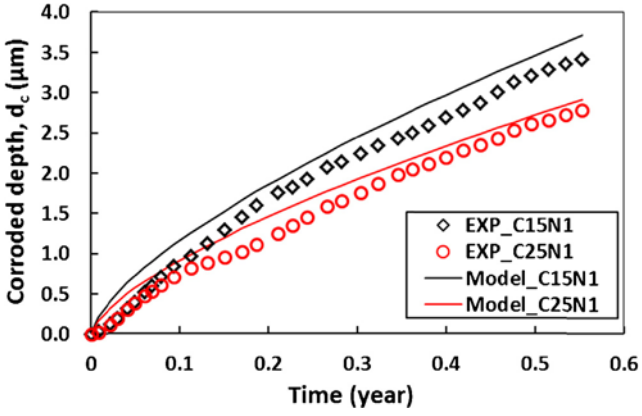

Fig. 10 – Corrosion modelling (Eq. (2)) of R/SHCC specimens with a single crack.

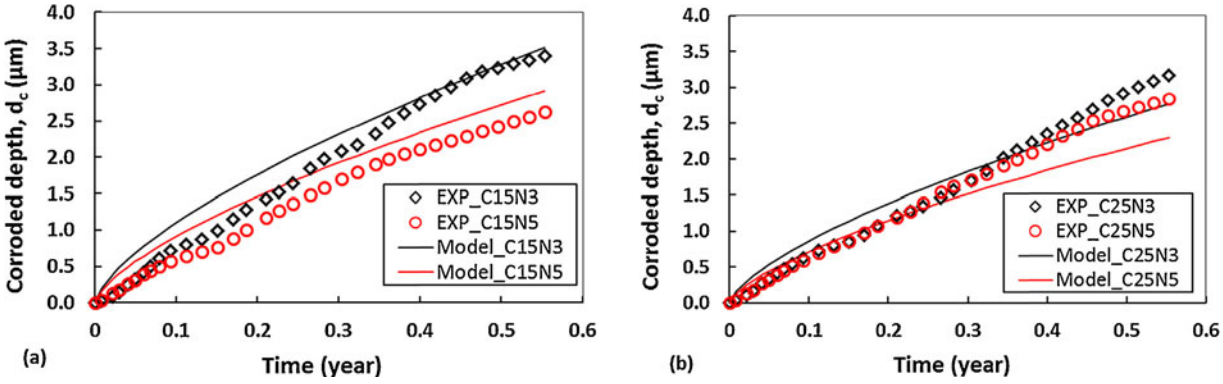

Fig. 11 – Corrosion modelling (Eq. (3)) of FS32 specimens containing 3 and 5 cracks, spaced 40 mm and 20 mm apart respectively with (a) 15 mm and (b) 25 mm cover to the steel bar.

Cl_{free} is the % of free chloride at the steel surface level (% wt of binder), S_{cr} is the average crack spacing in the specimen (mm) and C is the cover depth to the steel bar. δ_T and δ_{RH} are the factors that depend on the temperature and relative humidity (RH) at the steel bar level. At the specimen surface temperature of 21 ± 2 °C, δ_T can be considered to be 1. Similarly, for $55 \pm 5\%$ RH, δ_{RH} can be considered to be 1. α_t, α_{cl}, α_S and α_C are the factors that depend on the ratio of wetting and drying periods, types of binder, range of maximum crack spacing and quality of cover concrete, i.e. micro-structure and tensile strength of concrete. In this research work, the values of α_t, α_{cl}, α_S and α_C were considered to be 0.68, 0.5, 0.27 and 0.3 respectively. With these values, Fig. 10 shows reasonable agreement between Eq. (2) and the experimental data for single crack (notched) FS32 specimens, while in Fig. 11a and b Eq. (3) is shown to be in reasonable agreement with corroded depths in multiply cracked R/FS32 specimens. However, these values may need to be re-calibrated for other material types, exposure conditions, age and different corrosion rate measurement techniques. In both Figs. 10 and 11 the data points represent coulostatic corrosion rate measurements and application of Eq. (1).

Fig. 11a shows the corroded depths of R/FS32 specimens with 15 mm cover, and with three notches (N3) and five notches (N5) with corresponding crack spacing of 40 mm and 20 mm respectively. The larger crack spacing in N3 specimens was found to cause higher corroded depths in the steel bar. Fig. 11b shows a similar trend as in Fig. 11a for a 25 mm cover depth. The proposed corrosion model is valid for coulostatic measurement of the R/SHCC specimen corrosion rates in the laboratory experiments where the temperature (21 ± 2 °C) and RH ($55 \pm 5\%$) were controlled throughout the test period. For the different temperatures, RH and corrosion measuring methods, the proposed modelling may need to be calibrated.

6. Conclusions

This paper focusses on R/SHCC durability in terms of corrosion damage in embedded steel reinforcing bars under chloride exposure. The presentation of free and total chloride profiles, steel bar corrosion damage and its correlations with free chloride content, crack width and spacing in R/SHCC is novel. The following conclusions are drawn:

- The crack widths and crack spacing in R/FS31 specimens with 15 mm cover depth (C15) were larger than for larger cover depths C25 and C35. There was no significant difference in crack width and spacing between the C25 and C35 specimens.
- The average pitting depths in the steel bars are lower for R/SHCC specimens with a smaller crack spacing.
- The corroded depth in the steel bar is larger for higher free chloride content at the rebar level and larger crack widths.
- The free chloride content at the level of the steel bar surface is better correlated to corrosion damage than the total chloride content.
- The experimental results of chloride-induced corrosion in this paper can be represented by power functions incorporating average crack width, crack spacing, free chloride content at the steel surface and the time of exposure.

REFERENCES

[1] M.B. Otieno, M.G. Alexander, H.D. Beushausen, Corrosion in cracked and uncracked concrete – influence of crack width, concrete quality and crack reopening, Magazine of Concrete Research 62 (6) (2010) 393–404.
[2] C.Q. Li, S.T. Yang, Prediction of concrete crack width under combined reinforcement corrosion and applied load, Journal of Engineering Mechanics 137 (11) (2011) 722–731.
[3] T. Liu, R.W. Weyers, Modelling the dynamic corrosion process in chloride contaminated concrete structures, Cement and Concrete Research 28 (3) (1998) 365–379.
[4] T.U. Mohammed, N. Otsuki, M. Hisada, T. Shibat, Effect of crack width and bar types on corrosion of steel in concrete, Journal of Materials in Civil Engineering 13 (2001) 194–201.
[5] J.L. Granju, S. Balouch, Corrosion of steel fibre reinforced concrete from the cracks, Cement and Concrete Research 35 (3) (2005) 572–577.

[6] T. Vidal, A. Castel, R. Francois, Analyzing crack width to predict corrosion in reinforced concrete, Cement and Concrete Research 34 (1) (2004) 165–174.
[7] C. Arya, F.K. Ofori-Darko, Influence of crack frequency on reinforcement corrosion in concrete, Cement and Concrete Research 26 (3) (1996) 345–353.
[8] S.E. Hussain, A. Rasheeduzzafar, A.S. Al-Musallam, Al-Gahtani, Factors affecting threshold chloride for reinforcement corrosion in concrete, Cement and Concrete Research 25 (1995) 1543–1555.
[9] Q. Huang, Influence of Cracks on Chloride-induced Corrosion in Reinforced Concrete Structures, (M.Sc. thesis), Chalmers University of Technology, Sweden, 2006.
[10] C. Alonso, C. Andrade, M. Castellote, P. Castro, Chloride threshold values to depassivate reinforcing bars embedded in a standardized OPC mortar, Cement and Concrete Research 30 (2000) 1047–1055.
[11] P. Lambert, C.L. Page, P.R.W. Vassie, Investigation of reinforcement corrosion. Electrochemical monitoring of steel in chloride contaminated concrete, Materials and Structures 24 (1991) 351–358.
[12] O.A. Kayyali, M.N. Haque, The ratio of Cl/OH in chloride contaminated concrete. A most important criterion, Magazine of Concrete Research 47 (1995) 235–242.
[13] M. Thomas, Chloride thresholds in marine concrete, Cement and Concrete Research 26 (4) (1996) 513–519.
[14] F.H. Wittmann, P. Wang, P. Zhang, Z. Tie-Jun, F. Betzung, Capillary absorption and chloride penetration in neat and water repellent SHCC under imposed strain, in: Proceeding for 2nd International Conference on Strain Hardening Cementitious Composites, Brazil, (2011) 165–172.
[15] J.A. Gonzalez, A. Cobo, M.N. Gonzalez, S. Feliu, On-site determination of corrosion rate in reinforced concrete structures by use of galvanostatic pulses, Corrosion Science 43 (2001) 611–625.
[16] C. Andrade, C. Alonso, Test methods for on-site corrosion rate of steel reinforcing in concrete by means of the polarization resistance method, Materials and Structures 37 (9) (2004) 623–643.
[17] S.C. Paul, G.P.A.G. van Zijl, Crack formation and chloride induced corrosion in reinforced strain hardening cement-based composites (R/SHCC), Journal of Advanced Concrete Technology 12 (2014) 340–351.
[18] M. Sahmaran, V.C. Li, C. Andrade, Corrosion resistance performance of steel reinforced engineered cementitious composite beams, ACI Materials Journal 105 (3) (2008) 604–611.
[19] K. Kobayashi, T. Iizuka, H. Kurachi, K. Rokugo, Corrosion protection performance of high performance fibre reinforced cement composites as a repair material, Cement and Concrete Composites 32 (2010) 411–420.
[20] H. Mihashi, S.F.U. Ahmed, A. Kobayakawa, Corrosion of reinforcing steel in fibre reinforced cementitious composites, Journal of Advanced Concrete Technology 9 (2) (2011) 159–167.
[21] J. Broomfield, Corrosion of Steel in Concrete: Understanding, Investigating and Repair, Taylor & Francis, New York, 2007.
[22] S. Miyazato, Y. Hiraishi, Durability against steel corrosion of HPFRCC with bending cracks, Journal of Advanced Concrete Technology 11 (2013) 135–144.
[23] C. Alonso, C. Andrade, J.A. Gonzalez, Relation between resistivity and corrosion rate of reinforcements in carbonated mortar made with several cement types, Cement and Concrete Research 8 (5) (1988) 687–698.
[24] RILEM TC 178-TMC, Testing and modelling chloride penetration in concrete. Analysis of water soluble chloride content in concrete, Materials and Structures 35 (2002) 586–588.
[25] RILEM TC 178-TMC, Testing and modelling chloride penetration in concrete. Analysis of total chloride content in concrete, Materials and Structures 35 (2002) 583–585.
[26] G. Fischer, V.C. Li, Effect of fibre reinforcement on the response of structural members, in: Proc. of the Fracture Mechanics of Concrete and Concrete Structures, Vail, USA, (2004) 831–838.
[27] P. Schiessl, M. Raupach, Laboratory studies and calculations on the influence of crack width on chloride-induced corrosion of steel in concrete, ACI Materials Journal 94 (1) (1997) 56–61.
[28] S.C. Paul, The Role of Cracks and Chlorides in Corrosion of Reinforced Strain Hardening Cement-based Composite (R/SHCC), (Ph.D. thesis), Stellenbosch University, South Africa, 2015, , Available at http://scholar.sun.ac.za.
[29] A. Djerbi, S. Bonnet, A. Khelid, V. Baroghel-bouny, Influence of traversing crack on chloride diffusion into concrete, Cement and Concrete Research 38 (2008) 877–883.
[30] W.P. Boshoff, F. Altmann, C.J. Adendorff, V. Mechtcherine, A new approach for modelling the ingress of deleterious materials in cracked strain hardening cement-based composites, Materials and Structures (2015), http://dx.doi.org/10.1617/s11527-015-0649-8.